Static and Dynamic Structure of $Ru_3(CO)_9(\mu_3-\eta^2:\eta^2:\eta^2-C_6H_6)$ at Room Temperature and 193 K

Dario Braga* and Fabrizia Grepioni

Dipartimento di Chimica "G. Ciamician", Università di Bologna, Via Selmi 2, 40126 Bologna, Italy

Brian F. G. Johnson, Jack Lewis,* Catherine E. Housecroft,* and Marcia Martinelli

University Chemical Laboratory, University of Cambridge, Lensfield Road, Cambridge CB2 1EW, U.K.

Received July 20, 1990

The solid-state structure of the cluster benzene complex $Ru_3(CO)_9(\mu_3-\eta^2:\eta^2:\eta^2-C_6H_6)$ (1) has been determined at room temperature (RT) and 193 K (LT) by single-crystal X-ray diffractometry. 1 is monoclinic, space group $P2_1$, $Z = 2$, $a = 9.027$ (1) Å, $b = 12.665$ (2) Å, $c = 9.049$ (3) Å, $\beta = 118.15$ (2)° for RT and $a = 8.985$ (1) Å, $b = 12.527$ (2) Å, $c = 9.011$ (1) Å, $\beta = 118.217$ (9)° for LT. The benzene ligand shows a clear Kekulé-type distortion: "long" and "short" C–C bonds [1.45 (1), 1.40 (2) and 1.45 (1), 1.41 (1) Å for RT and LT, respectively] alternate within the C_6H_6 fragment, the short bonds being involved in the coordination to the metal atoms. The H atoms bend away from the metal frame [average bending 21.1° and 21.5° for RT and LT, respectively]. Insights into the structure and bonding in 1 are obtained by semiempirical Fenske–Hall calculations. The differences in solid-state structures between 1 and the osmium analogue $Os_3(CO)_9(\mu_3-\eta^2:\eta^2:\eta^2-C_6H_6)$ (2) are discussed in terms of intermolecular packing interactions. The molecular motion about the equilibrium position of 1 is studied by means of thermal motion analysis, while potential energy barrier calculations within the atom–atom approach are used to show that neither intramolecular nor intermolecular potential energy interactions oppose the reorientational motion of the benzene fragment in the solid state.

Introduction

$M_3(CO)_9(\mu_3-\eta^2:\eta^2:\eta^2-C_6H_6)$ (M = Ru, Os)[1,2] represent the prototype of an increasingly populated family of arene clusters. A remarkable feature of these complexes is the variety of bonding modes adopted by the benzene or its fragments. We now focus on derivatives that contain face-capping $(\mu_3-\eta^2:\eta^2:\eta^2-C_6H_6)$ ligands, for which only a few examples are known, namely $Ru_3(CO)_9(\mu_3-\eta^2:\eta^2:\eta^2-C_6H_6)$,[1] $Ru_6C(CO)_{11}(\mu_3-\eta^2:\eta^2:\eta^2-C_6H_6)(\eta^6-C_6H_6)$,[2] $Os_3(CO)_9(\mu_3-\eta^2:\eta^2:\eta^2-C_6H_6)$,[3] and $Os_3(CO)_8(\eta^2-CH_2CH_2)(\mu_3-\eta^2:\eta^2:\eta^2-C_6H_6)$.[4] A face-capping arene has also been observed in the cobalt derivative $[(CpCo)_3(\mu_3-\eta^2:\eta^2:\eta^2-C_6H_5CH{=}CHMe)]$.[5] It has been also found that the benzene ligand is able to migrate from a face-capping arene to terminal-bonding arene as in the case of $Os_3(CO)_7(\mu_3-\eta^2-Me_2C_2)(\eta^6-C_6H_6)$.[6] Terminal bonding of arenes in ruthenium clusters is known since the discovery of both carbide species $Ru_6C(CO)_{14}(Me_3C_6H_3)$[7] and is being found in both ruthenium species such as $Ru_6C(CO)_{14}(MeC_6H_5)$[8] and osmium species such as $H_2Os_4(CO)_{10}(\eta^6-C_6H_6)$.[9]

We now report the X-ray crystallographic characterization of $Ru_3(CO)_9(\mu_3-\eta^2:\eta^2:\eta^2-C_6H_6)$ at room temperature (RT) and 193 K (LT). The aims of this paper can be summarized as follows: (i) to provide a comparative analysis of the structure and bonding of $Ru_3(CO)_9(\mu_3-\eta^2:\eta^2:\eta^2-C_6H_6)$ with that of the osmium analogue $Os_3(CO)_9(\mu_3-\eta^2:\eta^2:\eta^2-C_6H_6)$; (ii) to discuss the differences in molecular organization between the crystal packings of the two species in terms of intramolecular and intermolecular interactions; (iii) to investigate the small amplitude motion about the equilibrium position of the $Ru_3(CO)_9(\mu_3-\eta^2:\eta^2:\eta^2-C_6H_6)$ molecule (and of its fragments) by means of thermal motion analysis; and (iv) to investigate the possibility of benzene reorientational motion in the solid state of the kind evidenced by spectroscopic techniques for other related benzene clusters. Potential energy barrier calculations based on the atom–atom approach (see below) are used for this procedure.

Results and Discussion

Structure of $Ru_3(CO)_9(\mu_3-\eta^2:\eta^2:\eta^2-C_6H_6)$. $Ru_3(CO)_9(\mu_3-\eta^2:\eta^2:\eta^2-C_6H_6)$ (1) crystallizes in the monoclinic space group $P2_1$ with one independent molecule in the asymmetric unit. The benzene molecule adopts a face-capping bonding mode over the Ru_3 triangle. ORTEP views down the benzene plane for both RT and LT structures are shown in Figure 1, parts a and b, respectively. Relevant bond distances and angles for the two determinations are reported in Table I. A comparative analysis of some relevant structural parameters of 1, of the Os analogue $Os_3(CO)_9(\mu_3-\eta^2:\eta^2:\eta^2-C_6H_6)$ (2), and of $Ru_3(CO)_{12}$[10] and $Os_3(CO)_{12}$[11] is reported in Table II.

(i) Benzene Ligand. The high quality of the data of 1 allows for an unambiguous description of the bonding between the ring and the underlying metal frame in terms of C–C bond length alternation. This is evident in both RT and LT determinations where "long" and "short" C–C bonds average 1.45 (1), 1.40 (2) and 1.45 (1), and 1.41 (1)

(1) Johnson, B. F. G.; Lewis, J.; Martinelli, M.; Wright, A. H.; Braga, D.; Grepioni, F. *J. Chem. Soc., Chem. Commun.* **1990**, 364.
(2) Gomez-Sal, M. P., Johnson, B. F. G.; Lewis, J.; Raithby, P. R. *J. Chem. Soc., Chem. Commun.* **1985**, 1682.
(3) Gallop, M. A.; Gomez-Sal, M. P.; Housecroft, C. E.; Johnson, B. F. G.; Lewis, J.; Owen, S. M.; Raithby, P. R.; Wright, A. H. *J. Am. Chem. Soc.*, in press.
(4) Gallop, M. A.; Johnson, B. F. G.; Lewis, J.; Raithby, P. R.; *J. Chem. Soc., Chem. Commun.* **1987**, 1809.
(5) Wadephol, H.; Buchner, K.; Protzkow, H. *Angew. Chem., Int. Ed. Engl.* **1987**, *26*, 1259.
(6) Braga, D.; Grepioni, F.; Martinelli, M.; Johnson, B. F. G.; Lewis, J. *J. Chem. Soc., Chem. Commun.* **1990**, 53.
(7) Sirigu, A.; Bianchi, M.; Benedetti, E. *J. Chem. Soc. D* **1969**, 596.
(8) Farrugia, L. J. *Acta Crystallogr.* **1988**, *C44*, 997.
(9) Cheng, H.; Johnson, B. F. G.; Lewis, J.; Braga, D.; Grepioni, F.; Parisini, E. *J. Chem. Soc., Dalton Trans.* **1991**, 215.
(10) Churchill, M. R.; Hollander, F. J.; Hutchinson, J. P. *Inorg. Chem.* **1977**, *16*, 2655.
(11) Churchill, M. R.; DeBoer, B. G. *Inorg. Chem.* **1977**, *16*, 878.

0276-7333/91/2310-1260$02.50/0

Table I. Relevant Bond Distance (Å) and Angles (deg) for 1 at Room Temperature (RT) and 193 K (LT)

	RT	LT		RT	LT
		Bond Distances			
Ru(1)-Ru(2)	2.829 (1)	2.828 (1)	Ru(2)-Ru(3)	2.827 (1)	2.827 (1)
Ru(1)-Ru(3)	2.855 (1)	2.855 (1)	mean	2.837 (1)	2.837 (1)
		Equatorial CO's			
Ru(1)-C(2)	1.92 (1)	1.92 (1)	C(3)-O(3)	1.13 (1)	1.14 (1)
Ru(1)-C(3)	1.91 (1)	1.92 (1)	C(4)-O(4)	1.12 (1)	1.16 (1)
Ru(2)-C(4)	1.92 (1)	1.91 (1)	C(5)-O(5)	1.12 (1)	1.15 (1)
Ru(2)-C(5)	1.91 (1)	1.90 (1)	C(7)-O(7)	1.10 (1)	1.15 (1)
Ru(3)-C(7)	1.92 (1)	1.89 (1)	C(8)-O(8)	1.14 (1)	1.14 (2)
Ru(3)-C(8)	1.91 (1)	1.91 (1)	mean Ru-C(CO)	1.92 (1)	1.91 (1)
C(2)-O(2)	1.12 (1)	1.14 (2)	mean C-O	1.12 (1)	1.15 (1)
		Axial CO's			
Ru(1)-C(1)	1.87 (1)	1.88 (1)	C(6)-O(6)	1.15 (1)	1.15 (1)
Ru(2)-C(6)	1.89 (1)	1.89 (1)	C(9)-O(9)	1.15 (1)	1.17 (1)
Ru(3)-C(9)	1.88 (1)	1.87 (1)	mean Ru-C	1.88 (1)	1.88 (1)
C(1)-O(1)	1.15 (1)	1.13 (1)	mean C-O	1.15 (1)	1.15 (1)
		Benzene			
Ru(1)-C(10)	2.348 (5)	2.346 (4)	C(12)-C(13)	1.37 (1)	1.40 (1)
Ru(1)-C(11)	2.287 (5)	2.288 (5)	C(13)-C(14)	1.45 (1)	1.45 (1)
Ru(2)-C(12)	2.377 (5)	2.379 (5)	C(14)-C(15)	1.41 (1)	1.41 (1)
Ru(2)-C(13)	2.306 (5)	2.303 (4)	C(10)-C(15)	1.44 (1)	1.45 (1)
Ru(3)-C(14)	2.356 (4)	2.359 (5)	mean Ru-C long	2.360 (5)	2.361 (5)
Ru(3)-C(15)	2.310 (5)	2.317 (5)	mean Ru-C short	2.301 (4)	2.303 (5)
C(10)-C(11)	1.41 (1)	1.41 (1)	mean C-C long	1.45 (1)	1.45 (1)
C(11)-C(12)	1.45 (1)	1.46 (1)	mean C-C short	1.40 (1)	1.41 (1)
C(10)-H(1)	0.93 (5)	0.90 (6)	C(13)-H(4)	0.93 (5)	0.91 (6)
C(11)-H(2)	0.89 (5)	0.90 (7)	C(14)-H(5)	0.90 (5)	0.90 (4)
C(12)-H(3)	0.93 (5)	0.93 (6)	C(15)-H(6)	0.90 (5)	0.89 (5)
			av C-H	0.91	0.91
		Bond Angles			
Ru(1)-C(1)-O(1)	171 (1)	172 (1)	Ru(2)-C(6)-O(6)	175 (1)	176 (1)
Ru(1)-C(2)-O(2)	176 (1)	177 (1)	Ru(3)-C(7)-O(7)	174 (1)	177 (1)
Ru(1)-C(3)-O(3)	177 (1)	176 (1)	Ru(3)-C(8)-O(8)	178 (1)	176 (1)
Ru(2)-C(4)-O(4)	178 (1)	178 (1)	Ru(3)-C(9)-O(9)	173 (1)	172 (1)
Ru(2)-C(5)-O(5)	177 (1)	178 (1)			
C(2)-Ru(1)-Ru(3)	122.6 (2)	122.7 (1)	C(5)-Ru(2)-Ru(3)	93.2 (2)	92.9 (1)
C(2)-Ru(1)-C(3)	94.4 (3)	94.9 (2)	C(7)-Ru(3)-Ru(2)	113.2 (2)	113.7 (2)
C(3)-Ru(1)-Ru(2)	85.0 (2)	84.5 (2)	C(7)-Ru(3)-C(8)	97.2 (3)	96.8 (2)
C(4)-Ru(2)-Ru(1)	111.4 (2)	111.8 (2)	C(8)-Ru(3)-Ru(1)	90.3 (2)	90.2 (1)
C(4)-Ru(2)-C(5)	95.0 (3)	94.8 (2)			
C(10)-C(11)-C(12)	118.2 (4)	119.5 (3)	C(13)-C(14)-C(15)	120.2 (4)	120.5 (3)
C(11)-C(12)-C(13)	121.7 (4)	120.7 (3)	C(14)-C(15)-C(10)	119.3 (4)	120.0 (3)
C(12)-C(13)-C(14)	119.5 (4)	119.3 (4)	C(15)-C(10)-C(11)	121.0 (4)	119.9 (4)

Table II. Comparison of Some Relevant Structural Parameters (Å) for 1, 2, $Ru_3(CO)_{12}$, and $Os_3(CO)_{12}$

	1[a]	2[b]	$Ru_3(CO)_{12}$[c]	$Os_3(CO)_{12}$[d]
M-M range	2.827 (1)-2.855 (1)	2.836 (1)-2.884 (1)	2.851 (1)-2.859 (1)	2.874 (1)-2.882 (1)
M-M av	2.837 (1)	2.857 (1)	2.855 (1)	2.877 (1)
M-CO eq[e] (av)	1.91 (1)	1.89 (3)	1.92 (1)	1.91 (1)
M-CO ax[f] (av)	1.88 (1)	1.90 (3)	1.94 (1)	1.95 (1)
C-O eq (av)	1.15 (1)	1.17 (4)	1.13 (1)	1.15 (1)
C-O ax (av)	1.15 (1)	1.14 (4)	1.13 (1)	1.13 (1)
M-C(C_6H_6) (av)	2.331 (4)	2.33 (3)		

[a] $Ru_3(CO)_9(C_6H_6)$. [b] $Os_3(CO)_9(C_6H_6)$, from ref 3. [c] From ref 10. [d] From ref 11. [e] Equatorial. [f] Axial.

Å, respectively, the short bonds being those interacting directly with the Ru atoms. The difference between the two sets of bonds is ca. 0.05 Å, as such being much smaller than that observed in the case of **2** [long 1.51 (4), short 1.41 (3) Å, Δ = 0.10 Å]. However, the poor quality of this latter data set makes this difference insignificant. It is important to note, instead, that Kekulê-type distortions have been clearly ascertained in species such as $(\eta^6\text{-}C_6H_6)Cr(CO)_3$[12] [1.423 (2), 1.406 (2) Å, Δ = 0.017 Å at 78 K] and $(\eta^6\text{-}C_6H_6)Mo(CO)_3$[13] [1.423 (2), 1.403 (1) Å, Δ = 0.020 Å at 120 K], and for the cluster complex $[(CpCo)_3(\mu_3\text{-}\eta^2\text{:}\eta^2\text{:}\eta^2\text{-}C_6H_5CH{=}CHMe)]$[5] [1.45 (1), 1.42 (1) Å, Δ = 0.03 Å] irrespective of the fact that the arene is singly or multiply coordinated to the metal centers.

The C-C-C angles within the ring are also alternatively smaller [mean 119.3 (4)°] and larger [mean 120.6 (5)°] than the ideal value of 120°. This small, but significant, difference is related to the Ru-C interactions, which also alternate in length [mean 2.361 (5) and 2.303 (5) Å, respectively], the short ones being with the C atoms showing closing up of the C-C-C angle. These deformations result

(12) (a) Rees, B.; Coppens, P. *Acta Crystallogr.* **1973**, *B29*, 2516. (b) Wang, Y.; Angermund, K.; Goddard, R.; Kruger, C. *J. Am. Chem. Soc.* **1987**, *109*, 587.

(13) Braga, D.; Grepioni, F.; Bürgi, H. B. *Inorg. Chem.*, submitted for publication.

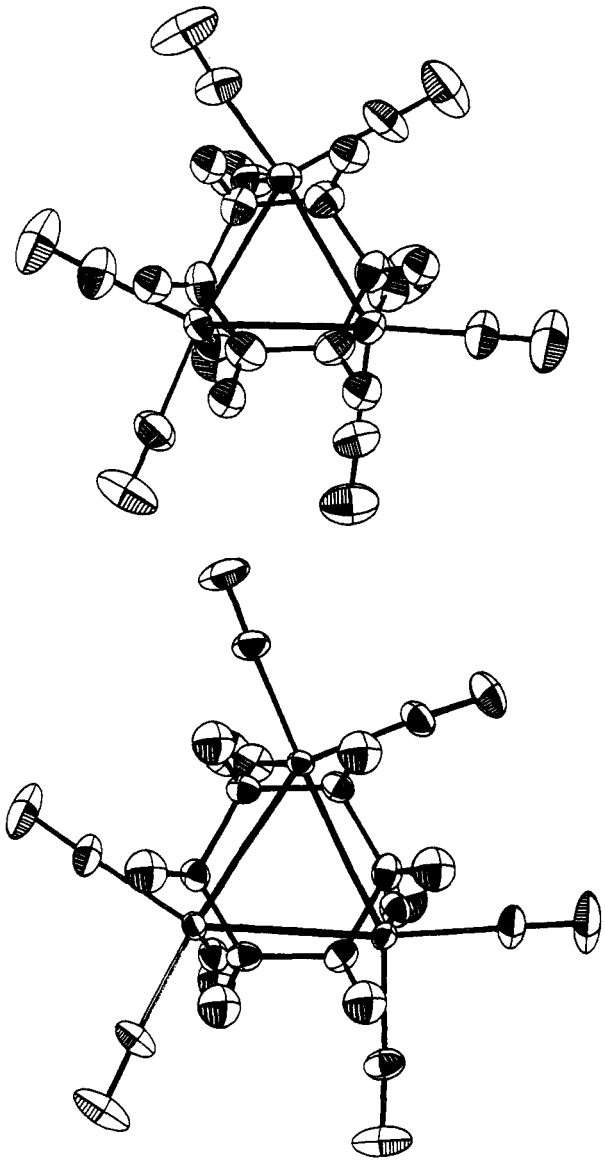

Figure 1. ORTEP drawings (50% probability) of the structure of 1 at room temperature (a, top) and 193 K (b, bottom).

in a slight tilt (approximately 4.5°) of the benzene moiety with respect to exact eclipsing of the double bond midpoints over the Ru atoms. A similar effect does not appear to be present in **2**, where Os–C(benzene) distances are more scattered [ranging from 2.27 (2) to 2.42 (2) Å] and do not follow a regular 3-fold pattern as in **1**. However, the Ru–C(benzene) and Os–C(benzene) distances are identical in their mean values [2.331 (4) and 2.33 (3) Å]. Of particular interest, in view of the ever-standing dispute on H-atom bending toward or away from the metal atoms in complexes of this kind, is the out-of-plane bending of the C–H bonds away from the metal atoms (average bending with respect to C_6 plane 21.1° and 21.5°, respectively; see also Figure 2). The C_6 and Ru_3 planes are almost exactly parallel (angle between planes 0.6 and 0.5°).

(ii) Metal Cluster. The metal triangle is only approximately equilateral: in both RT and LT structures, the Ru(1)–Ru(3) bond is slightly longer than the other two [2.855 (1) versus 2.827 (1) and 2.828 (1) Å].

The average value of 2.837 (1) Å in **1** is smaller than in $Ru_3(CO)_{12}$ [2.855 (1) Å], as it is in **2** with respect to $Os_3(CO)_{12}$ [2.857 (1) versus 2.877 (1) Å], the resulting "shrinkage" upon substitution of the benzene molecule for three axial CO's being approximately identical in **1** and

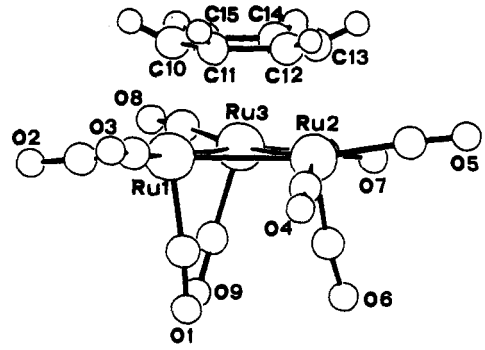

Figure 2. View of the structure of **1** showing the out-of-plane bending of the H atoms and the torsion of the $(CO)_3$ groups.

2 [0.018 and 0.020 Å, respectively]. This effect may be ascribed to the less efficient π-accepting capability of benzene with respect to three CO groups, which results in a slight increase of bonding electron density over the metal framework. As shown in Table II, the difference in metal frame sizes (in terms of metal–metal bond lengths) between the two benzene derivatives **1** and **2** and between the two corresponding binary carbonyls $Ru_3(CO)_{12}$ and $Os_3(CO)_{12}$ is almost identical [0.020 and 0.022 Å, respectively].

(iii) Carbonyl Groups. Each Ru atom bears a tricarbonyl unit constituted of two equatorial ligands and one axial CO ligand. The axial ligand shows slightly shorter Ru–C distances with respect to the equatorial ones [1.88 (1) versus 1.91 (1) Å in RT; 1.88 (1) versus 1.91 (1) Å in LT], indicative of an increased π-back-donation over the ligands trans to the benzene double bonds. Because of the different treatment of the thermal motion of the light atoms,[14] no direct comparison of the M–C and C–O distances is possible between **1** and **2**. It should be observed, however, that in $Ru_3(CO)_{12}$ the equatorial Ru–C distances are shorter than the axial ones [1.921 (5) and 1.942 (4) Å, respectively].

The most striking difference between the structures of **1** and **2** arises from the orientation of the $(CO)_3$ groups. While in **2** the equatorial ligands are substantially coplanar with the metal triangle and the axial ones are orthogonal to this plane, this is not the case for **1**. The torsion of the C_6 ring with respect to the Ru_3 triangle is reflected in alternate deviations above and below the cluster plane of the equatorial CO's and in a distortion from orthogonality of the axial ones [the average torsion of the $(CO)_3$ groups around their coordination axes, with respect to $Ru_3(CO)_{12}$, is ca. 10°].

Bonding in $Ru_3(CO)_6(\mu_3\text{-}\eta^2\text{:}\eta^2\text{:}\eta^2\text{-}C_6H_6)$. Fenske–Hall Calculations. Recently we described the bonding in $Os_3(CO)_9(\mu_3\text{-}\eta^2\text{:}\eta^2\text{:}\eta^2\text{-}C_6H_6)$, **2**, by using the Fenske–Hall quantum chemical method and modeling the cluster with $Ru_3(CO)_9(\mu_3\text{-}\eta^2\text{:}\eta^2\text{:}\eta^2\text{-}C_6H_6)$.[3] These results illustrated that the bonding of the benzene ring to the metal triangle may be described in terms of the Dewar–Chatt–Duncanson approach applicable to an alkene interacting with a single transition metal in low oxidation state. Thus, ligand-to-metal donation occurs primarily through the interaction of the degenerate HOMO of C_6H_6 with the degenerate LUMO (MO's 58 and 59) of the $Os_3(CO)_9$ framework (Figure 3a), while back-donation from the metal to the ligand involves the interaction of MO's 55 and 56 with the LUMO of C_6H_6 (Figure 3b). This analysis accounts satisfactorily for the alternation in C–C bond lengths con-

(14) (a) Braga, D.; Koetzle, T. F. *J. Chem. Soc., Chem. Commun.* **1987**, 144. (b) Braga, D.; Koetzle, T. F. *Acta Crystallogr.* **1988**, *B44*, 151.

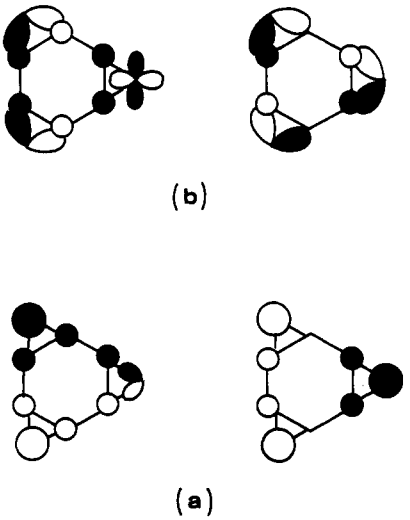

Figure 3. Interaction of the MO's of the $[Ru_3(CO)_9]$ and $[C_6H_6]$ fragments: (a) MO's 58/59 with the HOMO of C_6H_6 and (b) MO's 55/56 with the LUMO of C_6H_6.

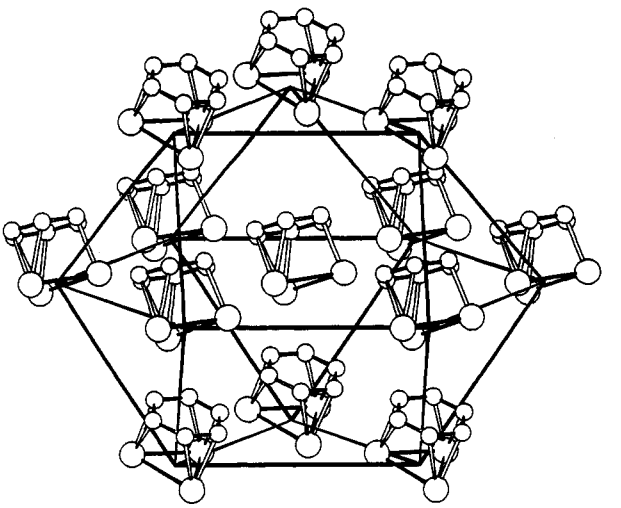

Figure 4. Anticuboctahedral distribution of the 12 molecules constituting the enclosure shell of 1. Carbonyl groups and H atoms are omitted for clarity.

firmed experimentally in 2. In addition, the calculations showed that the metal–benzene interfragment interaction was enhanced if the arene C–H vectors tilted away from the M_3 platform. In structurally characterizing 1, we have confirmed the nonplanarity of the organic ligand, but, significantly, the gross structure of 1 is not equivalent to that of its osmium analogue 2. A model compound that appears to be chemically reasonable [in this case $Ru_3(CO)_9(\mu_3\text{-}\eta^2\text{:}\eta^2\text{:}\eta^2\text{-}C_6H_6)$ in place of $Os_3(CO)_9(\mu_3\text{-}\eta^2\text{:}\eta^2\text{:}\eta^2\text{-}C_6H_6)$] is often used in molecular orbital calculations in order to reduce the atomic basis sets. Naturally then, if the model compound is later found to possess a different structure from that assumed, it throws into question the validity of the simplification. We have therefore examined the bonding in 1 by using the Fenske–Hall method.[3]

The results of the bonding analysis for 1 are as expected, and the interactions of the arene with the $\{Ru_3(CO)_9\}$ platform may be described in the same general terms as above. The principal difference is that the directionality of the frontier orbitals of the $\{Ru_3(CO)_9\}$ fragment reflects the fact that the carbonyl ligands are twisted with respect to those in the osmium analogue. Thus, given the experimentally determined geometry for 1, the orbital analysis appears to give a similar net bonding picture as we previously described in the model compound.

Why then does $Ru_3(CO)_9(\mu_3\text{-}\eta^2\text{:}\eta^2\text{:}\eta^2\text{-}C_6H_6)$ adopt a less symmetrical structure than $Os_3(CO)_9(\mu_3\text{-}\eta^2\text{:}\eta^2\text{:}\eta^2\text{-}C_6H_6)$? In an attempt to answer this question, we have considered the effect of rotating the benzene ligand through an angle α ($0 \leq \alpha \leq 10°$, experimental $\alpha = 4.5°$) with respect to a fixed trimetal framework which is isostructural with that observed for the $\{Os_3(CO)_9\}$ platform in 2. As the arene rotates, individual interfragment orbital interactions, which were optimized when $\alpha = 0°$, may begin to be "switched off". In order to prevent this, the metal-associated MO's must track the movement of the organic ligand.[15] Since the directionality of the frontier MO's of a metal fragment is controlled by the orientation of the carbonyl ligands, the necessity to retain good interfragment orbital overlap causes concomitant geometrical changes to the $\{Ru_3(CO)_9\}$ platform; i.e., a natural consequence of rotating the benzene ring is a twisting of the three $Ru(CO)_3$ units. This qualitative description is sufficient to rationalize why the overall asymmetry observed in 1 exists, but it is not able to explain why the distortion occurs in the first place.

Intramolecular and Intermolecular Interactions. As discussed above, 1 and 2 can be said to be isostructural only in the first approximation. In terms of idealized molecular symmetry, while 2 possesses clear C_{3v} symmetry, the idealized symmetry is reduced to C_3 in 1.

As shown above, these differences do not seem to arise from specific bonding requirements of the Ru species with respect to the Os analogue nor from the differences in metal carbonyls or metal–metal interactions, which are small and comparable to those observed between the isostructural (and isomorphous) species $Ru_3(CO)_{12}$[10] and $Os_3(CO)_{12}$.[11] Thus, we have to focus our attention on the "steric" effects, i.e., on the balance between intra- and intermolecular interactions.

(i) Intramolecular H–C(CO Equatorial) Interactions. The H–C(CO equatorial) interactions appear to be essentially repulsive in nature, as can be demonstrated by calculating the intramolecular potential energy barrier [ΔE(intra), see Computational Procedures below] for a rotation of the C_6H_6 fragment around an axis passing trough its center and the center of the Ru_3 triangle. The benzene fragment is found to "sit" halfway in between a minimum of the intramolecular potential (ca. −2.0 kcal·mol^{-1}, attainable by tilting the fragment up to C–Ru eclipsing) and a maximum (ca. 2.0 kcal·mol^{-1}, corresponding to the ideal superimposition of the C=C midpoints over the Ru atoms). This (rather rough) picture of the benzene–carbonyl steric interaction can be taken as indicative that intramolecular nonbonding effects favor the benzene ligand tilting (and, consequently, the torsion of the tricarbonyl groups) with respect to the more symmetric situation found in 2.

(ii) Intermolecular Interactions and Packing Arrangement. An appreciation of the intermolecular effects must be based on the knowledge of the molecular organization within the crystal lattice.

It is worth recalling that $Ru_3(CO)_{12}$ and $Os_3(CO)_{12}$ are isostructural and isomorphous,[10,11] while 1 and 2 crystallize in two different space groups.

We have recently developed[16] a method, based on potential energy calculations, to approach the crystal pack-

(15) A similar mutual "tracking" of the metal and ligand frontier orbitals has been noted in metalloborane complexes: DeKock, R. L.; Deshmukh, P., Fehlner, T. P.; Housecroft, C. E.; Plotkin, J. S.; Shore, S. G. *J. Am. Chem. Soc.* **1983**, *105*, 815.

(16) Braga, D.; Grepioni, F.; Sabatino, P. *J. Chem. Soc., Dalton Trans.* **1990**, 3137.

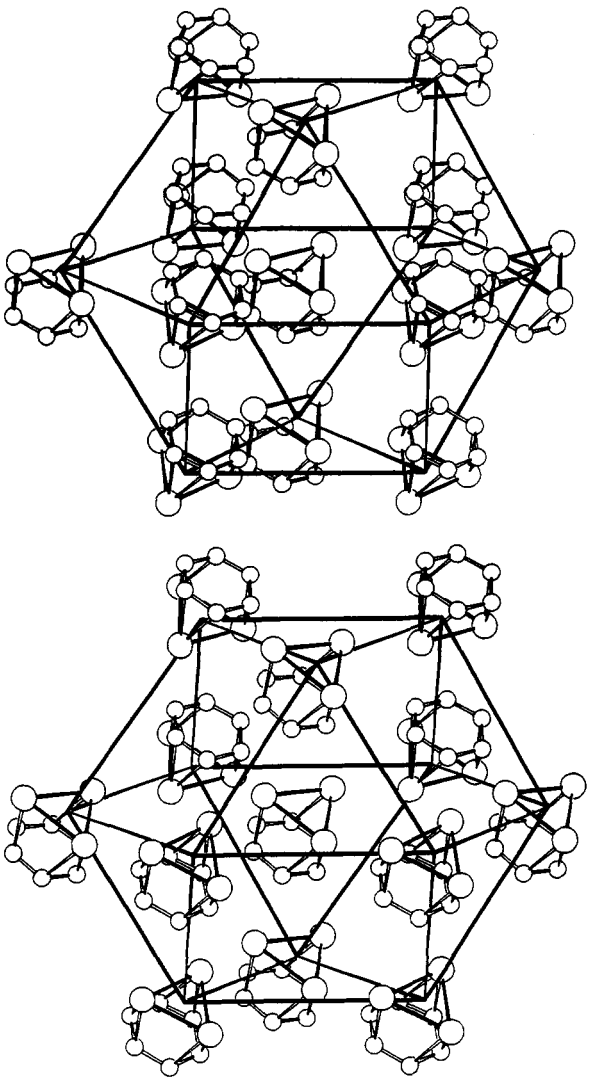

Figure 5. Cuboctahedral enclosure shells of **2**; (a, top) ES around the molecule in general position, (b, bottom) ES around the molecule bisected by the crystallographic mirror plane (ref 3). Carbonyl groups and H atoms are omitted for clarity.

ings of organometallic species in a way that focuses on the molecular organization *around* the molecule under examination (the reference molecule, RM). The method affords a simple and unambiguous picture of the packing pattern (the "enclosure shell", ES), thus allowing an easy appreciation of the intermolecular interactions.

The ES of **1** is depicted in Figure 4. As we have previously observed for the first-row metal carbonyls, the enclosure shell is constituted of 12 molecules (that is to say, close packing of roughly spherical molecules) forming an anti-cubooctahedral packing (A/B/A sequence of layers, h.c.p.).

The situation for **2** is complicated by the presence of "one and a half" molecules in the asymmetric unit of the space group *Im* (nonstandard setting of *Cm*), the second molecule being bisected by a crystallographic mirror plane. We have examined the ES's around both molecules in **2** (see Figure 5) and found that they not only differ around each molecule but do also differ substantially from that of **1**. In the case of **2**, the two sets of 12 molecules organize themselves in cubooctahedral ES's (A/B/C sequence of layers, c.c.p.). Moreover, the relative orientations of the molecules constituting the ES's with respect to the two RM's are different, thus confirming that the two molecular units in **2** experience different packing environments.

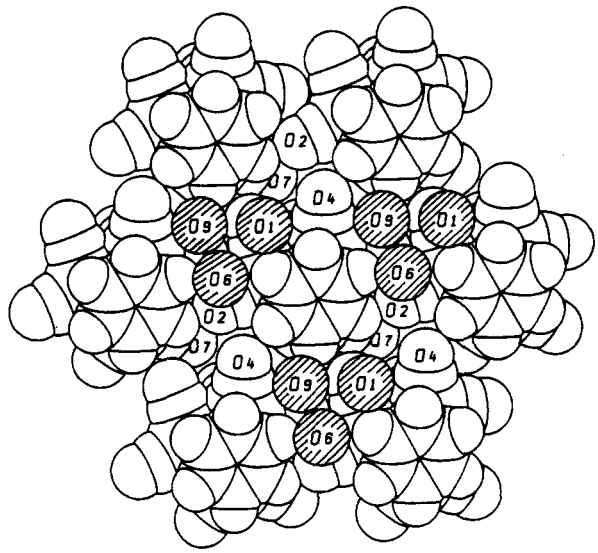

Figure 6. Space-filling projection of the molecules belonging to the central layer of the ES of **1**, showing the distribution around RM of the CO groups displaced above the plane [CO(2), CO(4), CO(7)] defined by the Ru_3 triangle (see Figure 2). Those displaced below the plane [CO(3), CO(5), CO(8)] are "hidden" underneath the axial ligands (shaded circles) "pushed in" from above.

Altogether, the molecular assembling in the crystals of **1** and **2** represent two alternative ways to achieve close packing.

The knowledge of the ES arrangement is essential to the understanding of the origin of the deformations observed in **1**. Figure 6 shows the organization of the molecules belonging to the central layer. It can be seen that the CO groups showing "out-of-plane" displacement [CO(2), CO(4), CO(7)] (as well as those showing downward displacement [CO(3), CO(5), CO(8)]), belonging to RM and to the surrounding molecules, group in 3-fold symmetry around RM. When a second layer is added above the central one (the three upper molecules in Figure 4), the axial CO's of these molecules are able to penetrate three of the six hollow sites left between the benzene groups. These sites correspond to the CO(3), CO(5), CO(8) groupings of equatorial ligands. Under the steric pressure of the axial ligands above, these ligands are "pushed down", causing the rotation of the entire tricarbonyl units. Therefore, the deformations observed in the solid-state structure of **1** seem to have mainly intermolecular origin: since $(CO)_3$ torsion *accompanied* by benzene tilting costs little to the bonding in **1**, the optimization of the intermolecular interactions (and, to some extent, of the intramolecular ones) becomes important.

As for the differences in structure *and* packing between **1** and **2**, the only conclusion that can be drawn is that the two **crystal structures** represent two alternative solutions to the problem of minimizing the "global" energy of the system. The crystals of **1** and **2** can be regarded as a special case of crystal polymorphism[17] in which the small differences caused by substitution of Ru for Os (but also the differences in crystallization conditions, solvents, etc.) can drive the crystallizaton process in one direction or the other. [On these premises, the possibility of existence of *true* polymorphic modifications of **1** or **2** can be envisaged and should be explored.]

Benzene Reorientation in Solid 1. We have previously shown[18] that the potential energy changes associated

(17) Bernstein, J. In *Organic Solid State Chemistry*; Desiraju, G. R., Ed.; Elsevier: Amsterdam, 1987; pp 471–510. Bernstein, J.; Hagler, A. T. *J. Am. Chem. Soc.* **1978**, *100*, 673.

with molecular fragment reorientational motions in solid neutral transition-metal complexes or clusters can be evaluated by the pairwise potential energy method (see also Computational Procedures for details).

In the case of the (arene) cluster species $Os_3(CO)_8(\eta^2\text{-}CH_2CH_2)(\mu_3\text{-}\eta^2\text{:}\eta^2\text{:}\eta^2\text{-}C_6H_6)$,[18c] this method has been fundamental in ascertaining the possibility of correlated motions of the two unsaturated fragments in the solid state in agreement with ^{13}C MAS NMR results.[19]

In the absence of spectroscopic information, the potential energy method has also proved to be useful in "predicting" reorientational behavior for the C_6H_6 fragment in solid $Os_3(CO)_7(Me_2C_2)(\eta^6\text{-}C_6H_6)$.[18c]

This is also the case of **1**, for which we have not been able, so far, to carry out solid-state NMR experiments due to the difficulty of preparing large quantities of the sample. However, a reorientational motion of the benzene fragment is plausible by analogy with the dynamic behavior shown by the aforementioned species.

The relative intermolecular potential energy profiles ΔE(inter) and ΔE(tot) [the sum of ΔE(inter) and ΔE(intra)] were calculated for a complete reorientation of the benzene fragment around an axis passing through the center of the C_6 ring and the center of the Ru_3 triangle at 10° rotational steps as described below in the Computational Procedures section. The ΔE profiles show minima of almost equal energy every 60°, corresponding to the idealized symmetry of the fragment. In **1**, ΔE(inter) values increase from 3.9 to 5.0 kcal·mol^{-1} on passing from RT to LT. ΔE(tot) retains the sinusoidal behavior though minima and maxima are shifted ca. 10° with respect to ΔE(inter), this being a consequence of the peculiarity of ΔE(intra) discussed above which does not place the observed structure (0° rotation) in a minimum of energy. ΔE(tot) barrier values increase from 4.5 to 6.3 kcal·mol^{-1} on passing from RT to LT.

These values are strictly comparable with those of the potential energy barriers to benzene reorientation at room temperature in $Os_3(CO)_8(\eta^2\text{-}CH_2CH_2)(\mu_3\text{-}\eta^2\text{:}\eta^2\text{:}\eta^2\text{-}C_6H_6)$ [5 kcal·mol^{-1}] and $Os_3(CO)_7(\mu_3\text{-}\eta^2\text{-}Me_2C_2)(\eta^6\text{-}C_6H_6)$ [2 kcal mol^{-1}][18c] as well as in the mononuclear species $(C_6H_6)Cr(CO)_3$ [4.6 and 7.5 kcal·mol^{-1} at RT and 78 K, respectively] and $(C_6H_6)_2Cr$ [2.0 and 3.9 kcal·mol^{-1} at RT and 100 K, respectively].[18b] These values were invariably found in good agreement with the activation energies/potential barriers yielded by spectroscopic techniques.

On these premises, it seems that the occurrence of benzene reorientation in solid **1** can be easily forecast.

Thermal Motion Analysis. Thermal motion analysis was carried out on the high-order data collected at 193 K [LTh] and on the full data set collected at room temperature [RTf]. The results are summarized in Table III. Rigid-body motion is described by the 12 nonvanishing elements of the **T**, **L**, and **S** (translational, librational, and screw) tensors.[20] The eigenvalues of the **L** (deg^2) and **T** (Å^2) tensors are reported in Table III.

First, a rigid-body (RB hereafter) motion of the whole $Ru_3(CO)_9(\mu_3\text{-}\eta^2\text{:}\eta^2\text{:}\eta^2\text{-}C_6H_6)$ molecule (with the exclusion of the H atoms) can be considered. It can be seen that both librational and translational motions, as shown by the eigenvalues of **L** and **T** tensors, are approximately isotropic and proportional to temperature. It is reasonable to expect, however, that the benzene and/or the carbonyl ligands possess additional motion with respect to the RB motion of the entire molecule. An in-plane librational motion can be predicted for the former, while the latter systems have been found to possess in related systems bending and torsional motions in the solid state.[13] These soft librational modes would be assorbed in the optimized RB parameters.[22]

Table III. Results of Rigid-Body Motion Analysis on the High-Order Data at 193 K (LTh) and on the Full Data Set at Room Temperature (RTf) for 1

	LTh	RTf
L_1, deg^2	8.8	14.1
L_2, deg^2	6.6	11.8
L_3, deg^2	5.4	9.8
T_1, 10^{-4} Å^2	157	280
T_2, 10^{-4} Å^2	149	269
T_3, 10^{-4} Å^2	127	242
$\langle\Delta U^2\rangle^{1/2}$, Å^2	6×10^{-4}	12×10^{-4}
$\langle\sigma^2(U)^{1/2}\rangle$, Å^2	25×10^{-4}	27×10^{-4}
wR[a]	0.068	0.054
Internally Moving Groups,[b] Motion around the Molecular Symmetry Axis		
rigid-body comp, deg^2	6.6	11.8
benzene additional motion	3.1 (2.0)	8.4 (3.4)
eq C(CO) additional motion	2.2 (0.7)	2.3 (1.4)
eq O(CO) additional motion	4.0 (0.9)	6.0 (1.2)
$\langle\Delta U^2\rangle^{1/2}$, Å^2	6×10^{-4}	11×10^{-4}
$\langle\sigma^2(U)^{1/2}\rangle$, Å^2	2×10^{-4}	0.049
Internally Moving Groups, Motion about the Coordination Axes of the Tricarbonyl Groups		
CO(1–3)		
rigid-body comp	5.6	10.1
C atoms additional motion	9.8	9.3
O atoms additional motion	10.1	18.3
CO(4–6)		
rigid-body comp	7.8	12.2
C atoms additional motion	0.8	−0.3
O atoms additional motion	6.9	9.3
CO(7–9)		
rigid-body comp	5.2	9.0
C atoms additional motion	10.0	18.6
O atoms additional motion	12.6	26.8
$\langle\Delta U^2\rangle^{1/2}$, Å^2	6×10^{-4}	11×10^{-4}
$\langle\sigma^2(U)\rangle^{1/2}$, Å^2	6×10^{-4}	27×10^{-4}

[a] $wR = [(\sum w(U_{obs} - U_{calc}))^2/(\sum(wU_{obs})^2)]^{1/2}$. [b] IMG's.

The THMA11 program[21] provides options to include these "internal" torsion modes (nonrigid body) in the thermal motion analysis. For each internal torsion mode, only one additional parameter is added, namely, the mean-square librational amplitude about a specified axis. The atoms expected to have some degree of additional motion constitute the internally moving groups (IMG's) in the analysis.

Three models of nonrigid body motion were examined, and the results are summarized in Table III.

(i) Internally Moving Benzene. The C_6 fragment is allowed additional librational freedom around an axis passing through its center of mass and the center of the Ru_3 triangle. The RB component increases from 6.6 deg^2 for LTh to 11.8 deg^2 for RTf. The benzene fragment shows a small additional motion for LTh (3.1 deg^2), which increases considerably (8.4 deg^2) on passing to RTf.

(ii) Internally Moving Equatorial CO's. In order to compare the librational freedom of the benzene fragment with respect to the equatorial CO's about the same axis,

(18) (a) Braga, D.; Gradella, C.; Grepioni, F. *J. Chem. Soc., Dalton Trans.* **1989**, 1721. (b) Braga, D.; Grepioni, F. *Polyhedron* **1990**, *1*, 53. (c) Braga, D.; Grepioni, F.; Johnson, B. F. G.; Lewis, J.; Martinelli, M. *J. Chem. Soc., Dalton Trans.* **1990**, 1847.

(19) Gallop, M. A.; Johnson, B. F. G.; Keeler, J.; Lewis, J.; Heyes, S. J.; Dobson, C. M. *J. Am. Chem. Soc.*, in press.

(20) Schomaker, V.; Trueblood, K. N. *Acta Crystallogr.* **1968**, *B21*, 63.

(21) Trueblood, K. N. THMA11 "Thermal Motion Analysis" Computer Program; University of California: Los Angeles.

(22) Dunitz, J. D.; Schomaker, V.; Trueblood, K. N. *J. Phys. Chem.* **1988**, *92*, 856. Bürgi, H. B. *Acta Crystallogr.* **1989**, *B45*, 383.

Table IV. Crystal Data and Details of Measurements for 1

	RT	LT
formula	$C_{15}H_6O_9Ru_3$	
M_r	633.4	
cryst size, mm	0.12 × 0.14 × 0.10	0.10 × 0.12 × 0.1
system	monoclinic	
space group	$P2_1$	
a, Å	9.027 (1)	8.985 (1)
b, Å	12.665 (2)	12.527 (2)
c, Å	9.049 (3)	9.011 (1)
β, deg	118.15 (2)	118.217 (9)
V, Å^3	912.2	893.7
Z	2	2
$F(000)$	600	
D_{calcd}, g cm^{-3}	2.31	2.35
λ(Mo Kα), Å	0.71069	
μ(Mo Kα), cm^{-1}	22.64	23.10
ϑ range, deg	2.5–35	2.5–40
ω scan width, deg	0.7	0.9
requested counting $\sigma(I)/I$	0.01	0.01
prescan rate, deg min^{-1}	5	3
prescan acceptance $\sigma(I)/I$	0.5	0.5
max scan time, s	120	120
range of reflns measd ($h_{min}h_{max}$,$k_{min}k_{max}$,$l_{min}l_{max}$)	−14,14;0,20;0,14	−16,16;0,22;0,16
measd reflns	3807	5910
abs correction[a] min, max values	0.90, 1.21	
unique obsd reflns used in the refinement $[F_o > 4\sigma(F_o)]$	3469	5363 (2771)
no. of refined params	264	264 (244)
R, R_w,[b] S	0.026, 0.031, 0.9	0.033, 0.035, 0.7 (0.031, 0.032, 1.5)
K, g[b]	1.0, 0.0018	1.0, 0.0036 (1.33, 0.0005)

[a] Absorption correction applied by the Walker and Stuart method.[25b] [b] $R_w = \sum[(F_o - F_c)w^{1/2}]/\sum(F_o w^{1/2})$, where $w = k/[\sigma(F) + |g|F^2]$. Values in parentheses refer to high-order refinement.

the C and O atoms of these ligands were grouped in two independent IMG's.

While the C atom extra motion is small and does not increase with temperature [2.2 and 2.3 deg^2 in LTh and RTf, respectively], the O atom extra motion is larger than the extra motion of the C atoms and increases with temperature [4.0 and 6.0 deg^2 in LTh and RTf, respectively].

(iii) Internally Moving $(CO)_3$ Groups. Finally, the possibility that the tricarbonyl groups might show some degree of torsional freedom around their coordination axes was explored. It can be noticed from Table III that the three $(CO)_3$ groups behave differently, although the RB components are almost identical (see Table IV) around the three different coordination axes. In all cases, the extra motion of the O atoms is larger than the extra motion of the C atoms, and they all increase with temperature. On the average (taking such an average of librational eigenvalues obtained in different reference systems for what it is worth), the C atoms of the CO groups, as well as the O atoms, appear to move more freely around the tricarbonyl group coordination axes than around the molecular symmetry C_3 axis.

The results of these observations can be summarized as follows:

(i) The molecule behaves as a rigid body in its motion about equilibrium only to a first approximation.

(ii) Both benzene and CO groups are internally moving with respect to the metal frame.

(iii) The librational freedom of benzene around the molecular C_3 axis is larger than that of the equatorial CO's.

(iv) The extra motion of the O atoms is always larger than that of the C atoms, indicating that some bending motion of the M–C–O axes is convoluted in the observed Us.

(v) There is a congruent increase of both rigid body and additional motions with temperature.

General Experimental Details

All reactions were performed under N_2 atmosphere by using standard Schlenk techniques, and the solvents were dried over the appropriate drying agents. Infrared spectra (IR) were recorded on a Perkin-Elmer 983 spectrometer using 0.1-mm solution cells, NMR spectra were recorded on a Bruker AM.400 spectrometer using the appropriate deuterated solvents, and their chemical shifts are reportd relative to $SiMe_4$. Electron-impact (EI) mass spectra were recorded at 70 eV (ca. 1.12×10^{-17} J) on an AEI MS12 instrument. Neutral products were purified by thin-layer chromatography (TLC) on 20-cm × 20-cm × 0.25-mm silica plates (Merck Kiesselgel $60F_{254}$).

$Ru_3(CO)_9(\mu_3\text{-}\eta^2\text{:}\eta^2\text{:}\eta^2\text{-}C_6H_6)$ is obtained by the following sequence of reactions:

(i) $[Ru_3(CO)_{10}(MeCN)_2]$. The bis(acetonitrile) complex was prepared by following the procedure established by Fould.[23] $[Ru_3(CO)_{12}]$ (500 mg) was dissolved in CH_2Cl_2 (250 mL) and MeCN (50 mL). A slight excess of a stoichiometric amount of Me_3NO (2.3 M equiv) in CH_2Cl_2 (50 mL) was added dropwise, and the reaction mixture was warmed up slowly from −78 °C to ambient temperature (20 °C). The reaction was monitored by IR, and when no more starting material was observed, the reaction mixture was filtered through silica and the solvent evaporated under reduced pressure and used immediately for the next reaction. IR ν_{CO} (THF): 2086 (w), 2055 (sh), 2018 (vs), 1999 (s), 1987 (sh), 1954 (m), 1819 (mw) cm^{-1}.

(ii) $[HRu_3(CO)_9(\mu_3\text{-}\eta^2\text{:}\sigma\text{:}\eta^2\text{-}C_6H_7)]$. $[Ru_3(CO)_{10}(MeCN)_2]$ was dissolved in benzene (250 mL). A large excess of 1,3-cyclohexadiene (1.5 mL) was added, and the mixture was heated to reflux for a period of 5–10 min. The solvent was evaporated under reduced pressure and the residue separated by TLC on silica plates using CH_2Cl_2 (30%) and hexane (70%). This reaction afforded the complex $[HRu_3(CO)_9(\mu_3\text{-}\eta^2\text{:}\sigma\text{:}\eta^2\text{-}C_6H_7)]$ (yield 150 mg, ca. 30%) as the major product, with $[Ru_3(CO)_9(\mu_3\text{-}\eta^2\text{:}\eta^2\text{:}\eta^2\text{-}C_6H_6)]$ (ca. 4%) and $[Ru_3(CO)_{12}]$ (40%). IR ν_{CO} (CH_2Cl_2): 2083 (m), 2055 (s), 2032 (vs), 2008 (m, br), 1958 (m) cm^{-1}. ^{1}H NMR δ ($CDCl_3$): 4.93 (1 H, t), 4.04 (2 H, dd), 3.68 (1 H, dd), 2.95 (2 H, d) 2.17 (1 H, d), −21.16 (1 H, d). MS m/z: 638 (as required).

(iii) $[HRu_3(CO)_9(\mu_3\text{-}\eta^2\text{:}\eta^2\text{:}\eta^2\text{-}C_6H_6)][BF_4]$. $[Hru_3(CO)_9(\mu_3\text{-}\eta^2\text{:}\sigma\text{:}\eta^2\text{-}C_6H_7)]$ was dissolved in CH_2Cl_2 (5 mL), and then a large excess of Ph_3CBF_4 was added. The mixture was allowed to react for 15–30 min at room temperature until the cation precipitated. The excess solvent was removed with a pipet. The fine precipitate was rinsed with CH_2Cl_2 (2 mL) and hexane (2 mL) and finally dried under reduced pressure. The precipitate was used in the next reaction without any further purification. This reaction showed quantitative conversion from $[HRu_3(CO)_9(\mu_3\text{-}\eta^2\text{:}\sigma\text{:}\eta^2\text{-}C_6H_7)]$ to the cation $[HRu_3(CO)_9(\mu_3\text{-}\eta^2\text{:}\eta^2\text{:}\eta^2\text{-}C_6H_6)]^+$. IR ν_{CO} (MeNO): 2115 (w), 2091 (s), 2068 (vs), 2049 (m) cm^{-1}. ^{1}H NMR δ (acetone-d_6): 6.10 (6 H, s), −20.11 (1 H, s).

(iv) $[Ru_3(CO)_9(\mu_3\text{-}\eta^2\text{:}\eta^2\text{:}\eta^2\text{-}C_6H_6)]$. The cation $[HRu_3(CO)_9(\mu_3\text{-}\eta^2\text{-}\eta^2\text{:}\eta^2\text{-}C_6H_6)][BF_4]$ was dissolved in CH_2Cl_2 (3 mL). A diluted solution of DBU (1,8-diazabicyclo[5.4.0]undec-7-ene) in CH_2Cl_2 was added dropwise, and the mixture was allowed to react until no more starting material was present. The solution was filtered through silica to remove any excess of DBU present. The solvent was evaporated under reduced pressure, and the products were separated by TLC using a mixture of CH_2Cl_2 (30%) and hexane as eluent, affording $[Ru_3(CO)_9(\mu_3\text{-}\eta^2\text{:}\eta^2\text{:}\eta^2\text{-}C_6H_6)]$ (yield 128 mg, ca. 85%) and a very small amount of $[Ru_3(CO)_{12}]$. IR ν_{CO} (CH_2Cl_2): 2071 (m), 2017 (vs), 1996 (s), 1976 (s, sh) cm^{-1}. ^{1}H NMR δ ($CDCl_3$): 4.56 (6 H, s). MS m/z 636.

X-ray Structure Determination. All X-ray measurements were made on an Enraf-Nonius CAD-4 diffractometer equipped with a graphite monochromator (Mo Kα radiation, λ = 0.71069 Å) and a Nonius low-temperature device, operating with liquid

(23) Fould, G. A.; Johnson, B. F. G.; Lewis, J. *J. Organomet. Chem.* 1985, *296*, 147.

Table V. Fractional Atomic Coordinates for 1 at 193 K

atom	x	y	z
Ru(1)	0.35985 (2)	0.72920	0.83990 (3)
Ru(2)	0.14629 (3)	0.71765 (3)	0.99021 (2)
Ru(3)	0.02546 (2)	0.64617 (3)	0.65536 (2)
C(1)	0.4022 (5)	0.5832 (3)	0.8314 (5)
O(1)	0.4447 (6)	0.4978 (3)	0.8278 (7)
C(2)	0.4958 (4)	0.7633 (4)	0.7367 (5)
O(2)	0.5849 (5)	0.7826 (5)	0.6816 (6)
C(3)	0.5347 (4)	0.7542 (3)	1.0650 (5)
O(3)	0.6402 (5)	0.7622 (4)	1.1987 (5)
C(4)	0.2432 (6)	0.7869 (4)	1.2040 (5)
O(4)	0.3067 (9)	0.8278 (6)	1.3354 (5)
C(5)	−0.0552 (5)	0.6761 (3)	0.9957 (5)
O(5)	−0.1721 (5)	0.6479 (4)	1.0011 (7)
C(6)	0.2770 (4)	0.5933 (3)	1.0872 (4)
O(6)	0.3514 (5)	0.5188 (3)	1.1520 (5)
C(7)	−0.2086 (5)	0.6137 (4)	0.5440 (6)
O(7)	−0.3494 (5)	0.5896 (5)	0.4793 (8)
C(8)	0.0685 (7)	0.6087 (3)	0.4750 (4)
O(8)	0.1037 (9)	0.5853 (4)	0.3715 (6)
C(9)	0.0704 (4)	0.5142 (3)	0.7675 (4)
O(9)	0.0812 (6)	0.4291 (3)	0.8193 (5)
C(10)	0.1853 (4)	0.8586 (2)	0.6493 (4)
C(11)	0.2546 (4)	0.8986 (3)	0.8142 (4)
C(12)	0.1554 (5)	0.8955 (2)	0.9027 (4)
C(13)	−0.0109 (4)	0.8568 (3)	0.8231 (4)
C(14)	−0.0829 (4)	0.8184 (3)	0.6511 (4)
C(15)	0.0115 (4)	0.8206 (3)	0.5649 (4)
H(1)	0.226 (6)	0.879 (6)	0.580 (4)
H(2)	0.337 (8)	0.947 (6)	0.851 (6)
H(3)	0.172 (5)	0.956 (4)	0.968 (7)
H(4)	−0.087 (4)	0.883 (6)	0.854 (5)
H(5)	−0.196 (6)	0.812 (7)	0.596 (5)
H(6)	−0.032 (5)	0.812 (7)	0.454 (6)

nitrogen. The intensities where collected in $\omega/2\vartheta$ scan mode at room temperature and at 193 (±0.5) K from two different crystal specimens. Crystal data and details of measurements for the two data collections are summarized in Table IV. The RT structure was solved by using direct methods followed by difference Fourier syntheses and subsequent least-squares refinement. The resulting coordinates were used in turn as the starting point for the refinement of the low-temperature data. Both analyses were based on scattering factors for neutral atoms taken from the *International Tables for X-ray Crystallography*.[24] For all calculations, the SHELX76 program was used.[25] Difference maps calculated from both full data sets showed weak peaks at expected H atom positions. These positions were refined with constraints on the C–H distances. One thermal parameter was refined for all H atoms [0.07 and 0.04 Å^2 for RT and 193 K, respectively]. All atoms but the hydrogen ones were refined anisotropically.

The high-order refinement of the LT data (LTh in Table 3) was performed with $\sin(\vartheta/\lambda)_{min} = 0.48$.

Fractional atomic coordinates for the LT refinement are reported in Table V; those for the RT refinement were previously deposited at the Cambridge Crystallographic Data Centre.[1]

Computational Procedures. Packing Potential Energy Calculations. The packing potential energy (ppe) of a neutral organometallic crystal can be evaluated within the atom–atom pairwise potential energy method[26] by means of the expression

$$\text{ppe} = \sum_i \sum_j [A \exp(-Br_{ij}) - Cr_{ij}^{-6}]$$

where r_{ij} represents the nonbonded atom–atom intermolecular distance. Index i in the summation runs over all atoms of one molecule (chosen as RM) and index j over the atoms of the surrounding molecules distributed according to crystal symmetry. A cutoff of 10 Å has been adopted in our calculations. The values of the coefficients A, B, and C used in this work are listed in Table VI.[27] The Ru atoms, for which such coefficients are not available, are treated as the corresponding noble gas (Xe). Ionic contributions are not considered.

Table VI. Parameters for the Atom–Atom Potential Energy Calculations[a]

	A, kcal mol^{-1}	B, Å^{-1}	C, kcal mol^{-1} Å^{-6}
H···H	4900	4.29	29.0
C···C	71600	3.68	421.0
O···O	77700	4.18	259.4
Ru···Ru[b]	372900	3.03	8373.0

[a] For crossed interactions: $A = (A_xA_y)^{1/2}$, $B = (B_x + B_y)/2$, $C = (C_xC_y)^{1/2}$. [b] Ru···Ru interactions were treated as Xe···Xe interactions (see text).

We have found that this choice of potential coefficients performs well when dealing with mononuclear or polynuclear organometallic complexes containing only, O, C, and H atoms besides the metal ones.

The results of ppe calculations are used to investigate the molecular packing arrangement around the RM. First, the separate contributions to ppe of all the molecules (usually in number from 40 to 60), generated around RM by space group symmetry within the cutoff distance of 10 Å, are calculated. Then the first-neighboring molecules (those constituting the ES) are selected among the surrounding molecules on the basis of the highest number of intermolecular contacts with RM (i.e., those that contribute most to ppe). This procedure ensures that all relevant contributions to ppe are taken into account.

It should be stressed, however, that the pairwise potential energy method is used herein *only* as a means (more efficient than others, though) to investigate the spatial distribution of the molecules around the one chosed as reference, with no pretentions of obtaining "true" crystal potential energy values. Details of the application of the method to organometallic crystals are given in ref 16 and 18.

Potential Energy Barrier Calculations. The Buckingham potential discussed above can also be used to evaluate the potential energy barriers associated with the benzene ligand reorientational motion over the cluster surface in 1. Because the basic assumption of the pairwise potential energy method is adopted,[26] namely that the interatomic interactions depend on the distances between the atomic nuclei, the H atoms were "moved" along the C–H vectors from the observed distances to the ideal value of 1.08 Å (thus retaining the correct orientations). Benzene reorientation was performed around the axis passing through the middle of the C_6 rings and the center of the Ru triangle. The potential energy was calculated at 10° rotational steps for a complete rotation of the fragment between ±180°. *Relative* potential energy profiles (ΔE) were calculated as ΔE = pe − pe(min), where pe(min) is the value corresponding to the observed structure (0° rotation). The intermolecular [ΔE(inter)] and intramolecular [ΔE(intra)] contributions were calculated separately. ΔE(tot) was obtained as ΔE(inter) + ΔE(intra). No cooperation or relaxation of the molecules surrounding the reorienting fragment was allowed ("static environment" approximation).

Packing potential energy and potential energy barrier calculations were performed by using a slightly modified version of the computer program OPEC.[28]

Acknowledgment. We thank Ms. S. Ribani for her help with the manuscript. Financial support by Consiglio Nazionale delle Ricerche is acknowledged.

Registry No. 1, 128363-71-3; $Ru_3(CO)_{12}$, 15243-33-1; MeCN,

(24) *International Tables for X-ray Crystallography*; Kynoch Press: Birmingham, England, 1975; Vol. IV, pp 99–149.
(25) (a) Sheldrick, G. M. SHELX76, Program for Crystal Structure Determination; University of Cambridge: Cambridge, England, 1976. (b) Walker, N.; Stuart, D. *Acta Crystallogr.* **1983**, *B39*, 158.
(26) (a) Pertsin, A. J.; Kitaigorodski, A. I. *The atom–atom potential method*; Springer-Verlag: Berlin, 1987. (b) Gavezzotti, A.; Simonetta, M. *Organic Solid State Chemistry*; Desiraju, G. R., Ed.; Elsevier: New York, 1987.
(27) (a) Gavezzotti, A. *Nouv. J. Chim.* **1982**, *6*, 443. (b) Mirsky, K. *Computing in Crystallography, Proceedings of the International Summer School on Crystallographic Computing*; Delft University Press: Twente, 1978; p 169. (c) Gavezzotti, A.; Simonetta, M. *Chem. Rev.* **1981**, *82*, 1.
(28) Gavezzotti, A. OPEC Organic Packing Potential Energy Calculations; University of Milano: Italy. See also: Gavezzotti, A. *J. Am. Chem. Soc.* **1983**, *195*, 5220.

75-05-8; $Ru_3(CO)_{10}(MeCN)_2$, 103257-53-0; $[HRu_3(CO)_9(\mu_3\text{-}\eta^2\text{:}\sigma\text{:}\eta^2\text{-}C_6H_7)]$, 128363-70-2; $[HRu_3(CO)_9(\mu_3\text{-}\eta^2\text{:}\eta^2\text{:}\eta^2\text{-}C_6H_6)][BF_4]$, 128391-81-1; 1,3-cyclohexadiene, 592-57-4.

Supplementary Material Available: Complete listings of positional and thermal parameters, atomic coordinates, and bond distances and bond angles for LTf and LTh (22 pages); listings of calculated and observed structure factors for LTf and LTh (49 pages). Ordering information is given on any current masthead page.

Synthesis and Chemistry of $Cp_2Zr(Ph)(THF)^+$. Selectivity of Protolytic and Oxidative Zr–R Bond-Cleavage Reactions

Samuel L. Borkowsky, Richard F. Jordan,* and Garry D. Hinch

Department of Chemistry, University of Iowa, Iowa City, Iowa 52242

Received September 24, 1990

The neutral complexes $Cp_2Zr(R)_2$ (R = CH_3 (1), CH_2Ph (2)) react with $[Cp'_2Fe][BPh_4]$ in THF via oxidative Zr–R bond cleavage to yield $[Cp_2Zr(R)(THF)][BPh_4]$ (R = CH_3 (3), R = CH_2Ph (4)). No reaction is observed with $Cp_2Zr(Ph)_2$ (5). The mixed phenyl–alkyl complexes $Cp_2Zr(Ph)(R)$ (R = CH_3 (9), CH_2Ph (10)) react with Cp'_2Fe^+ in THF to yield 3 and $Cp_2Zr(Ph)(THF)^+$ (6), respectively. The susceptibility of Zr–CH_2Ph bonds to oxidative cleavage is ascribed to the low bond energy. Reaction of 5 with $[HN(CH_3)_2Ph][BPh_4]$ in THF also produces 6 in good yield. Complexes 1, 2, and 5 react with $[HN(CH_3)_3][BPh_4]$ to yield $[Cp_2Zr(R)(OCH_2CH_2CH_2CH_2N(CH_3)_3][BPh_4]$ (R = CH_3 (15), CH_2Ph (13), and Ph (12)) via Zr–R bond protonolysis and subsequent nucleophilic THF ring opening. Reactions of 10 and 9 with $[HN(CH_3)_3][BPh_4]$ yield 13 and 15 via initial selective Zr–Ph protonolysis. Complex 1 reacts with $[HN(^nBu)_3][BPh_4]$ in THF to yield 3 whereas neither 2 nor 5 react. The selectivity and qualitative rates of these reactions indicate that ease of Zr–R bond protonolysis varies in the order Zr–Ph > Zr–CH_3 > Zr–CH_2Ph and that steric effects also strongly influence reactivity. Complex 6 reacts rapidly with 2 equiv of PMe_3 in THF solvent to yield $Cp_2Zr(Ph)(PMe_3)_2^+$ (16) and with 2-methylpyridine (α-picoline) in CD_2Cl_2 solvent to yield $Cp_2Zr(\eta^2(N,C)$-picolyl)$(THF)^+$ (17). Complex 6 initiates the ring-opening polymerization of THF and does not react with 2-butyne in CD_2Cl_2.

Current interest in the chemistry of $Cp_2M(R)(L)^+$ (M = Ti, Zr, Hf) complexes[1-3] is motivated by the proposed role of closely related 14-electron $Cp_2M(R)^+$ ions in Cp_2MX_2-based Ziegler–Natta olefin polymerization catalyst systems[4] and by the potential utility of these complexes in catalytic C–H activation/C–C coupling chemistry.[5] Cationic zirconium alkyl complexes of this type have been prepared by oxidative cleavage (with Ag^+, Cp_2Fe^+, or Cp'_2Fe^+ ($Cp' = C_5H_4Me$)) or protonolysis (with HNR_3^+) of Zr–R bonds of neutral Cp_2ZrR_2 complexes.[2,3] Related Ti cations have also been prepared by halide displacement reactions of $Cp_2Ti(CH_3)X$ in coordinating solvents, protonolysis of $Cp^*_2TiR_2$ and by one-electron oxidation of $Cp^*_2Ti(R)$.[1] In all these cases noncoordinating anions such as BPh_4^- are required for the isolation of stable salts.[6]

This paper describes the reactions of several symmetric Cp_2ZrR_2 and mixed $Cp_2Zr(R)(R')$ complexes with Cp_2Fe^+ and HNR_3^+ reagents. The principal objective of this study was to develop a simple synthesis of cationic phenyl complexes $Cp_2Zr(Ph)(L)^+$, which are of interest for structural and reactivity comparisons to other $Cp_2Zr(R)(L)^+$ complexes. Additionally, we were interested in elucidating the general reactivity and selectivity trends of these reactions with the ultimate objective of developing efficient methods for in situ generation of $Cp_2Zr(R)(L)^+$ catalysts.[5a] Several nucleophilic THF ring-opening reactions of $Cp_2Zr(R)(THF)^+$ complexes that we discovered during the course of these studies are also described.

Results

Reaction of $Cp_2Zr(Ph)(R)$ Complexes with Cp_2Fe^+ Reagents. Synthesis of $Cp_2Zr(Ph)(THF)^+$ from

(1) Ti complexes: (a) Bochmann, M.; Wilson, L. M.; Hursthouse, M. B.; Short, R. L. *Organometallics* **1987**, *6*, 2556. (b) Bochmann, M.; Wilson, L. M.; Hursthouse, M. B.; Motevalli, M. *Organometallics* **1988**, *7*, 1148. (c) Taube, R.; Krukowka, L. *J. Organomet. Chem.* **1988**, *347*, C9. (d) Bochmann, M.; Jagger, A. J.; Wilson, L. M.; Hursthouse, M. B.; Motevalli, M. *Polyhedron* **1989**, *8*, 1838. (e) Bochmann, M.; Jagger, A. J.; Nicholls, J. C. *Angew. Chem., Int. Ed. Engl.* **1990**, *29*, 780.

(2) Zr complexes: (a) Hlatky, G. G; Turner, H. W.; Eckman, R. R. J. *Am. Chem. Soc.* **1989**, *111*, 2728. (b) Jordan, R. F.; Dasher, W. E.; Echols, S. F. *J. Am. Chem. Soc.* **1986**, *108*, 1718. (c) Jordan, R. F.; Bagjur, C. S.; Willett, R.; Scott, B. *J. Am. Chem. Soc.* **1986**, *108*, 7410. (d) Jordan, R. F.; Echols, S. F. *Inorg. Chem.* **1987**, *26*, 383. (e) Jordan, R. F.; LaPointe, R. E.; Bajgur, C. S.; Echols, S. F.; Willett, R. *J. Am. Chem. Soc.* **1987**, *109*, 4111. (f) Jordan, R. F.; Bajgur, C. S.; Dasher, W. E.; Rheingold, A. L. *Organometallics* **1987**, *6*, 1041. (g) Jordan, R. F. *J. Chem. Educ.* **1988**, *65*, 285. (h) Jordan, R. F.; LaPointe, R. E.; Bradley, P. K.; Baenziger, N. C. *Organometallics* **1989**, *8*, 2892. (i) Jordan, R. F.; LaPointe, R. E.; Baenziger, N. C.; Hinch, G. D. *Organometallics* **1990**, *9*, 1539. (j) Jordan, R. F.; Bradley, P. K.; Baenziger, N. C.; LaPointe, R. E. *J. Am. Chem. Soc.* **1990**, *112*, 1289. (k) For a review, see: Jordan, R. F.; Bradley, P. K.; LaPointe, R. E.; Taylor, D. F. *New J. Chem.* **1990**, *14*, 505. (l) Turner, H. W.; Hlatky, G. G. European Patent Appl. 0 277 003, 1988. (m) Turner, H. W. European Patent Appl. 0 277 004, 1988.

(3) For related Th chemistry, see: Lin, Z.; LeMarechal, J.-F.; Sabat, M.; Marks, T. J. *J. Am. Chem. Soc.* **1987**, *109*, 4127.

(4) (a) Dyachkovskii, F. S.; Shilova, A. K.; Shilov, A. E. *J. Polym. Sci. Part C* **1967**, *16*, 2333. (b) Eisch, J. J.; Piotrowski, A. M.; Brownstein, S. K.; Gabe, E. J.; Lee, F. L. *J. Am. Chem. Soc.* **1985**, *107*, 7219. (c) Gassman, P. G.; Callstrom, M. R. *J. Am. Chem. Soc.* **1987**, *109*, 7875. (d) Gianetti, E.; Nicoletti, G. M.; Mazzocchi, R. *J. Poly. Sci., Polym. Chem. Educ.* **1985**, *23*, 2117. (e) Ewen, J. A. *J. Am. Chem. Soc.* **1984**, *106*, 6355. (f) Toscano, P. J.; Marks, T. J. *J. Am. Chem. Soc.* **1985**, *107*, 653. (g) Hedden, D.; Marks, T. J. *J. Am. Chem. Soc.* **1988**, *110*, 1647. (h) Dahmen, K.-H.; Hedden, D.; Burwell, R. L., Jr.; Marks, T. J. *Langmuir* **1988**, *4*, 1212. (i) Zambelli, A.; Longo, P.; Grassi, A. *Macromolecules* **1989**, *22*, 2186. (j) Pino, P.; Cioni, P.; Wei, J. *J. Am. Chem. Soc.* **1987**, *109*, 6189. (k) Ewen, J. A.; Jones, R. L.; Razavi, A.; Ferrara, J. D. *J. Am. Chem. Soc.* **1988**, *110*, 6255.

(5) (a) Jordan, R. F.; Taylor, D. F. *J. Am. Chem. Soc.* **1989**, *111*, 778. (b) Jordan, R. F.; Taylor, D. F.; Baenziger, N. C. *Organometallics* **1990**, *9*, 1546. (c) Jordan, R. F.; Guram, A. S. *Organometallics* **1990**, *9*, 2116. (d) Guram, A. S.; Jordan, R. F. *Organometallics* **1990**, *9*, 2190. (e) Guram, A. S.; Jordan, R. F. *J. Am. Chem. Soc.* **1990**, *113*, 1833.

(6) Anions such as PF_6^-, BF_4^-, $CF_3SO_3^-$, etc. react with or coordinate strongly to $Cp_2Zr(R)^+$ ions. See: (a) Jordan, R. F. *J. Organomet. Chem.* **1985**, *294*, 321. (b) Roddick, D. M.; Heyn, R. H.; Tilley, T. D. *Organometallics* **1989**, *8*, 324. (c) Martin, B. D.; Matchett, S. A.; Norton, J. R.; Anderson, O. P. *J. Am. Chem. Soc.* **1985**, *107*, 7952. (d) Siedle, A. R.; Newmaark, R. A.; Gleason, W. B.; Lammanna, W. M. *Organometallics* **1990**, *9*, 1290.

0276-7333/91/2310-1268$02.50/0